Optimal Control of Wastegate Throttle and Fuel Injection for a Heavy-Duty Turbocharged Diesel Engine During Tip-In

Kristoffer Ekberg[1]   Viktor Leek[1]   Lars Eriksson[1]

[1]Vehicular Systems, Dept. of Electrical Engineering, Linköping University, Sweden, `{kristoffer.ekberg,` `viktor.leek, lars.eriksson}@liu.se`

Abstract

The diesel engine remains one of the key components in the global economy, transporting most of the worlds goods. To cope with stricter regulations and the continuous demand for lower fuel consumption, optimization is a key method. To enable mathematical optimization of the diesel engine, appropriate models need to be developed. These are preferably continuously differentiable, in order to be used with a gradient-based optimization solver. Demonstration of the optimization-based methodology is also necessary in order for the industry to adapt it. The paper presents a complete mean value engine model structure, tailored for optimization and simulation purposes. The model is validated using measurements on a heavy-duty diesel engine. The validated model is used to study the transient performance during a time-optimal tip-in, the results validate that the model is suitable for simulation and optimization studies.

Keywords: Diesel Engine Modeling, Diesel Engine Control, Mean Value Models, Optimal Control, Optimization, Tip-in.

1   Introduction

The diesel engine is one of the prime movers of the global economy (Smil, 2010). It propels everything from cargo ships to passenger cars, and helps sustain modern life as we know it. Over the years, diesel emission regulations have become more and more strict, but it seems as the pace is not fast enough. Urban air pollution possibly caused by vehicle emissions, has led to major cities now saying they will ban diesel engines completely (Harvey, 2016). Zero-emission vehicles, benefiting from electrification, is one potential way of solving the emissions problem. However, the solution to the problem still lies in the future while diesel engines continues to be used today. It is therefore important that the diesel engine continues to be improved in order to reduce the environmental impact, local emissions, and fuel consumption. However, making improvements on a diesel powertrain is not a trivial task. Firstly, the diesel engine itself is very complex, and combining it with modern aftertreatment systems makes it considerably more complex because of the symbiotic dependence between the two systems. The engine needs the aftertreatment system to meet the regulations and the aftertreatment system needs heat from the engine to reduce the emissions. Secondly, more than 120 years of continuous development has led to the fact that the low-hanging fruits have already been picked. To overcome this, and continue to develop the diesel engine, there is a demand for new and different methodologies. Such a methodology that is starting to gain acceptance within the automotive industry is *optimization*. Together with modeling and simulation, it can help balance conflicting interests, such as keeping the aftertreatment warm while maintaining a low fuel consumption. For the transition to optimization-based methodologies to work, models suitable for optimization are needed, which is the focus of this paper. In it, a continuously differentiable heavy-duty diesel engine model, suitable for use with gradient-based optimization software is developed, and a simple use-case, showing how it can be used in an optimization framework, is demonstrated.

The developed model is a so-called mean value engine model, which is a control-based model for the study of the air and fueling system. The model is developed from stationary measurements on a heavy duty diesel engine and has four states, intake manifold pressure, exhaust manifold pressure, pressure after the compressor, turbocharger speed. The system also has three actuator inputs, fuel injection per cycle, throttle position, and wastegate position. Also, since there is no load connected to the engine model, the engine speed is treated as an exogenous input into the system, meaning that it is set from outside the model, which enables studying the engine under load conditions.

For a comprehensive treatment of modeling diesel engines for optimal control, the reader is referred to Asprion (2013), and for the modeling of hybrid electric powertrains for optimal control the reader is referred to Sivertsson (2015). Numerical optimal control is extensively treated in Betts (2010); Biegler (2010). For the solution of the optimal control problems in this paper, a toolbox called YOP[†] is used. It is based on CasADi (Andersson, 2013), which is a general symbolic framework for dynamic optimization. The resulting nonlinear program (NLP) from the optimal control algorithm is solved using the general NLP-solver IPOPT (Wächter, Andreas and Biegler, Lorenz T., 2006). Similar optimal control prob-

---

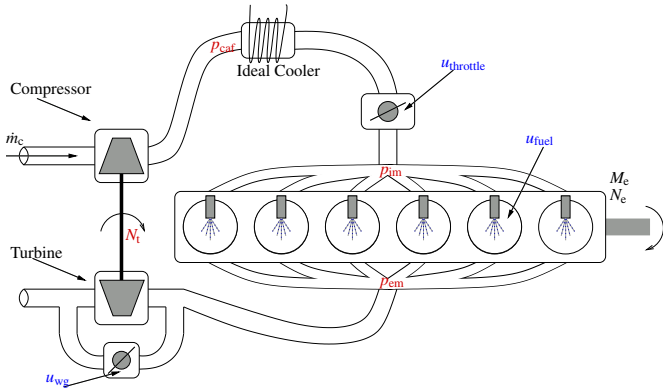[†]Contact the authors for more information about YOP.

Figure 1. Sketch of a diesel engine equipped with turbocharger, charge air cooler, throttle and wastegate. The model states are pressure after compressor p_{caf}, pressure in the intake manifold p_{im}, pressure in the exhaust manifold p_{em} and turbocharger rotational speed N_t. The charge air cooler is assumed to be ideal, therefore there is no pressure drop from the compressor to the throttle.

Symbol	Description	Unit
$\dot{m}$	Massflow	kg/s
n_r	Revolutions per stroke	-
p	Pressure	Pa
q_{hv}	Fuel Lower heating value	J/kg
q_{in}	In-cylinder specific heat	J/kg
r_c	Compression ratio	-
t	Time	s
u_{fuel}	Injected fuel	mg/cycle
u_{wg}	Wastegate position	-, $[0,1]$
u_{thr}	throttle position	-, $[0,1]$
A	Area	m^2
BSR	Blade speed ratio	-
C_d	Drag coefficient	-
J	Rotational inertia	$kg\,m^2$
M	Torque	Nm
N	Rotational speed	rpm
$\bar{N}$	Normalized rotational speed	rpm
P	Power	W
R	Gas constant	J/(kg K)
T	Temperature	K
V	Volume	m^3
W	Work	J
γ	ratio of specific heats	-
η	Efficiency	-, $[0,1]$
λ	Air-fuel equivalence ratio	-
ϕ	Fuel-air equivalence ratio	-
$(A/F)_s$	Air-Fuel stoichiometry relation	-
ψ	Flow condition function	-
ω	Angular velocity	rad/s
Π	Pressure ratio	-

Table 1. List of Symbols

lems, as studied in this paper, have previously been solved in for example Nezhadali and Eriksson (2016), Sivertsson and Eriksson (2014), and Leek et al. (2017).

The paper is outlined as follows. In Section 3 the model is presented and validated sub-model by sub-model. In Section 4 an optimal control problem for optimizing the transient response, for a tip-in, is formulated. In Section 5 the problem is solved numerically and the results presented. In Section 6 the conclusions are presented.

The contributions are, a complete model structure for a heavy-duty diesel engine equipped with a fixed geometry turbocharger and inlet throttle, and optimal control trajectories for a parametrization of the model during a tip-in.

2 Model

The model is intended to be used for controller design and evaluation of, both controller structures and control strategies. To reduce computational time when simulating the model, the number of states is kept low. The model is a mean value engine model, a model structure suitable for study of the air and fueling system of the engine. The sub-models are parametrized using sum of least squares method, the results from the parametrization's are shown as R^2 of the model fit, displayed in the figure title of each model that is adapted to measurement data.

2.1 States

The model states is described by four dynamic equations

$$\frac{dp_{caf}}{dt} = \frac{R_a\,T_{amb}}{V_{cac}}\left(\dot{m}_c - \dot{m}_{thr}\right) \tag{1a}$$

$$\frac{dp_{im}}{dt} = \frac{R_a\,T_{amb}}{V_{im}}\left(\dot{m}_{thr} - \dot{m}_{air}\right) \tag{1b}$$

$$\frac{dp_{em}}{dt} = \frac{R_e\,T_{em}}{V_{em}}\left(\dot{m}_{air} + \dot{m}_{fuel} - \dot{m}_t - \dot{m}_{wg}\right) \tag{1c}$$

$$\frac{d\omega_t}{dt} = \frac{1}{J_{tc}\,\omega_t}\left(P_t\eta_t - P_c\right), \tag{1d}$$

and consequently has four states $x = [p_{caf}\ p_{im}\ p_{em}\ \omega_t]^T$. It also has three actuator inputs $u = [u_{fuel}\ u_{thr}\ u_{wg}]$, and one exogenous input, the engine speed N_e.

2.2 Control Signals

The control signals in the model are the amount of fuel injected in the cylinders u_{fuel} in [mg/cycle], the wastegate control signal u_{wg} in a range from 0 to 1 [-], the throttle

Index	Description
a	Air
amb	Ambient
cac	Charge air cooler
caf	Compressor after
ch	Choke line
c	Compressor
$corr$	Corrected
$crit$	Critical
cyl	Cylinder
d	Displacement (cylinder)
D	Displacement (engine)
des	Desired
e	Engine
em	Exhaust manifold
f	Final
$fric$	Friction
ig	Indicated gross
ign	Ignition
im	Intake manifold
lin	Linear
ref	Reference
sc	Seiliger cycle
thr	Throttle
t	Turbine
vol	Volumetric
zsl	Zero-slope line

Table 2. List of subscripts

control signal u_{thr} in a range from 0 to 1 [-], and the engine speed N_e in [rpm]. The engine speed is treated as an exogenous input to be able to investigate the engine behavior in different load and speed conditions without having a driveline model.

2.3 Engine

The engine model is divided into four sub models; one for engine torque, one for cylinder air charge, one for engine stoichiometry, and one for exhaust temperature.

2.3.1 Engine Torque

The torque delivered by the combustion engine (Eriksson and Nielsen, 2014) is described by

$$\dot{m}_{fuel} = \frac{u_{fuel} N_e n_{cyl} 10^{-6}}{n_r} \tag{2a}$$

$$W_{pump} = V_d n_{cyl} (p_{em} - p_{im}) \tag{2b}$$

$$W_{ig} = \frac{\eta_{ign} \dot{m}_{\text{fuel}} q_{HV} n_r}{N_e} \left(1 - r_c^{1-\gamma_{cyl}}\right) \tag{2c}$$

$$W_{fric} = V_d n_{cyl} \left(c_{\text{fr}1} + c_{\text{fr}2} \frac{N_e}{1000} + c_{\text{fr}3} \left(\frac{N_e}{1000}\right)^2\right) \tag{2d}$$

$$M_e = \frac{W_{ig} - W_{pump} - W_{fric}}{2\pi n_r} \tag{2e}$$

where the parameters η_{ig}, $c_{\text{fr}1}$. $c_{\text{fr}2}$ and $c_{\text{fr}3}$ are model parameters. The control signal is the fuel flow u_{fuel} and the engine rotational speed N_e, expressed in rps.

2.3.2 Engine Air Massflow

The amount of fresh air entering the cylinders is dependent of the pressure in the intake manifold p_{im} and the engine rotational speed N_e (Eriksson and Nielsen, 2014).

$$\dot{m}_{cyl} = \frac{\eta_{vol} p_{im} N_e V_D}{n_r 60 R_a T_{im}} \tag{3a}$$

$$\eta_{vol} = c_{\text{vol}1} \sqrt{p_{im}} + c_{\text{vol}2} \sqrt{N_e} + c_{\text{vol}3} \tag{3b}$$

Where $c_{\text{vol}1}$, $c_{\text{vol}2}$, and $c_{\text{vol}3}$ are model parameters.

2.3.3 Air-to-Fuel Equivalence Ratio

The air-to-fuel equivalence ratio λ is described by

$$\lambda = \frac{\dot{m}_{air}}{\dot{m}_{fuel}(A/F)_s} \tag{4}$$

where $(A/F)_s$ is the stoichiometric air to fuel ratio.

2.3.4 Exhaust Gas Temperature

The exhaust gas temperature from the engine cylinders is needed to get the correct power to the turbine. The gas temperature leaving the cylinders and entering the exhaust manifold is described in a similar way as Skogtjärn (2002), but by an ideal diesel cycle (constant pressure during combustion), with a correction parameter η_{sc} which is a compensation factor for non ideal cycles.

$$q_{in} = \frac{\dot{m}_{fuel} q_{HV}}{\dot{m}_{fuel} + \dot{m}_{air}} \tag{5a}$$

$$T_{em} = \eta_{sc} \left(\frac{p_{em}}{p_{im}}\right)^{\frac{\gamma_{air}-1}{\gamma_{air}}} r_c^{1-\gamma_{cyl}} \left(\frac{q_{in}}{c_{p,air}} + T_{im} r_c^{\gamma_{air}-1}\right) \tag{5b}$$

The model validation for models (2)-(5) is displayed in Figure 2. Since the charge air cooler after the compressor is assumed to be ideal, the inlet manifold temperature $T_{im} = T_{amb}$.

2.4 Turbocharger

The compressor model consists of two parts, the first models the compressor air massflow, and the second the compressor efficiency.

2.4.1 Compressor Massflow

The compressor massflow model is developed in Leufvén and Eriksson (2013) and further described in Eriksson and Nielsen (2014). The model used in this paper is the representation from Eriksson and Nielsen (2014), described as
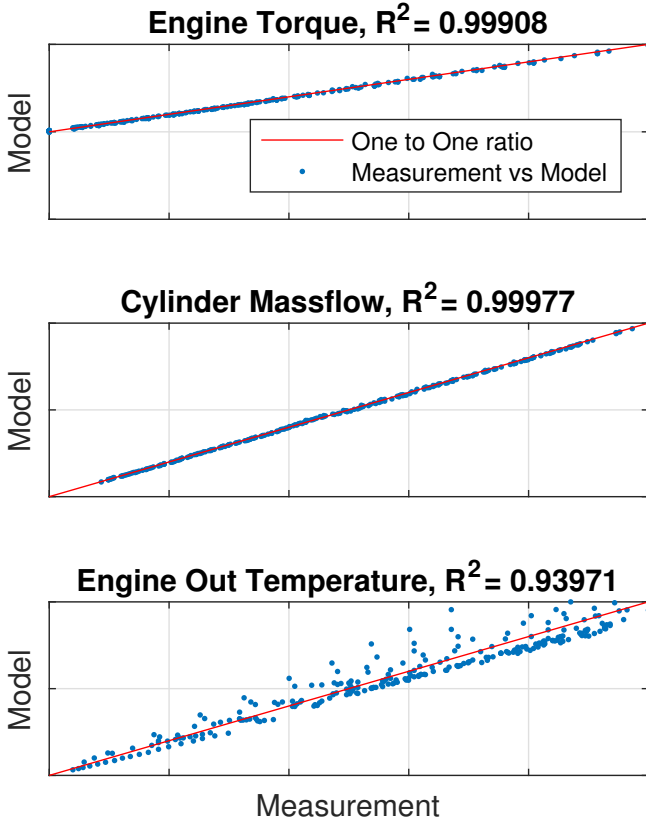
Figure 2. Model validation, blue dots represent measurement plotted against model, and the red line represents the line indicating an exact fit.
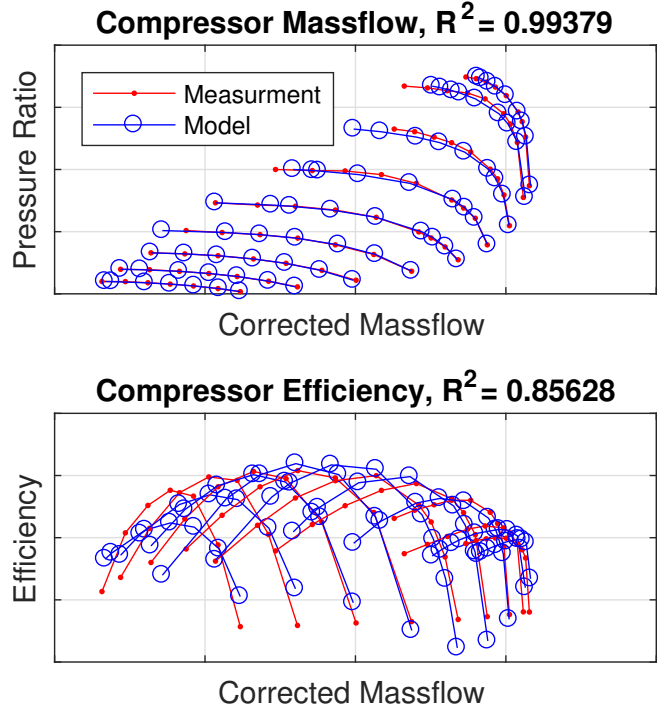

Figure 3. Compressor model validation, the measurement data (red) is compared with the massflow model (plot above) and the efficiency model (plot below), the models output data is shown in blue.

$\dot{m}_{c,corr}$ and the pressure ratio over the compressor Π_c. The model is described as

$$\chi = \begin{pmatrix} \sqrt{\Pi_c - 1} - \sqrt{\Pi_c^{max} - 1} \\ \dot{m}_{c,corr} - \dot{m}_{c,corr}^{max} \end{pmatrix} \qquad (8a)$$

$$\eta_c = \eta_c^{max} - \chi^T Q \chi \qquad (8b)$$

where Q is a symmetric positive definite matrix. In Figure 3, the model output is compared to the measured data.

2.4.3 Turbine Massflow

The turbine model (9) is found in Eriksson and Nielsen (2014), but (9b) has been extended to get a better model fit. The model output is compared to measured data in Figure 4, where it is seen, that the estimation of the turbine massflow is better at higher expansion ratios. When the turbocharger speed is higher, the estimation at lower expansion rations gets less accurate.

$$\Pi_t = \frac{p_{amb}}{p_{em}} \qquad (9a)$$

$$k_0 = c_{20} + c_{21} N_t + c_{22} N_t^2 \qquad (9b)$$

$$\Pi_0 = c_{10} + c_{11} N_t^{c_{12}} \qquad (9c)$$

$$\dot{m}_t = k_0 \sqrt{1 - (\Pi_t - \Pi_0)^{k_1}} \qquad (9d)$$

2.4.4 Compressor Out Temperature

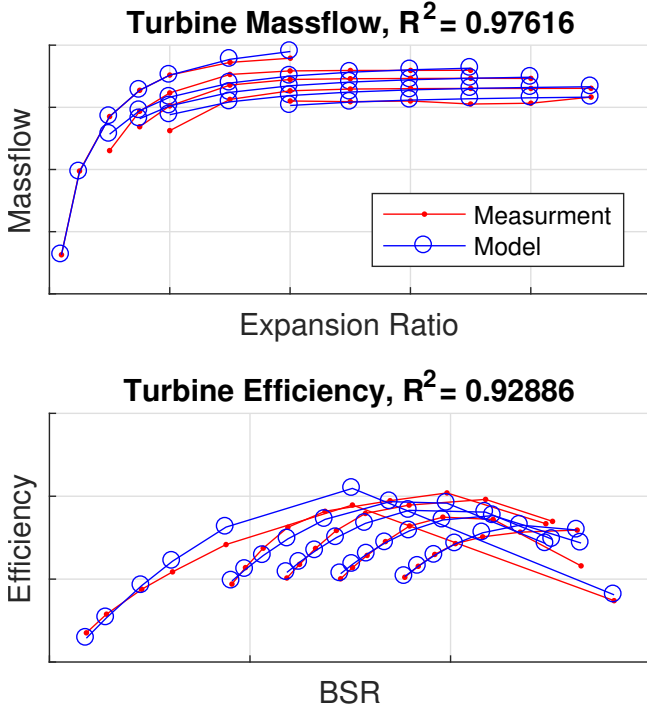The compressor outlet temperature is calculated by using the inlet air temperature, the assumption of an isentropic

$$\bar{N} = N_t / 10^5 \qquad (6a)$$

$$\Pi_{zsl} = 1 + c_{11} \bar{N}^{c_{12}} \qquad (6b)$$

$$\dot{m}_{zsl} = c_{20} + c_{21} \bar{N} + c_{22} \bar{N}^2 \qquad (6c)$$

$$\Pi_{ch} = c_{30} + c_{31} \bar{N}^{c_{32}} \qquad (6d)$$

$$\dot{m}_{ch} = c_{40} + c_{41} \bar{N}^{c_{42}} \qquad (6e)$$

$$C = c_{50} + c_{51} \bar{N} + c_{52} \bar{N}^2 \qquad (6f)$$

$$\dot{m}_{c,corr} = \dot{m}_{zsl} + (\dot{m}_{ch} - \dot{m}_{zsl}) \left(1 - \left(\frac{\Pi_c - \Pi_{ch}}{\Pi_{zsl} - \Pi_{ch}} \right)^C \right)^{\frac{1}{C}}. \qquad (6g)$$

There are 14 model parameters to estimate, the complete model fit is displayed in Figure 3. Equation (7) is used to translate the corrected massflow to massflow in $[kg/s]$.

$$\dot{m}_c = \dot{m}_{c,corr} \frac{p_{amb}}{p_{ref}} \sqrt{\frac{T_{ref}}{T_{amb}}} \qquad (7)$$

where p_{amb} and T_{amb} are the pressure and temperature in the compressor inlet, p_{ref} and T_{ref} are the reference pressure and temperature for which the compressor is tested.

2.4.2 Compressor Efficiency

The compressor efficiency model (Eriksson and Nielsen, 2014) has two inputs, the corrected compressor massflow

Turbine Massflow, R^2 = 0.97616

Turbine Efficiency, R^2 = 0.92886

Figure 4. Turbine model validation, the measurement data (red) is compared with the turbine massflow model (plot above) and the turbine efficiency model (plot below), the output data from the models is shown in blue.

compression, and the compressor efficiency. (Eriksson and Nielsen, 2014)

$$T_c = T_{amb} + \frac{T_{amb}}{\eta_c} \left(\Pi_c^{\frac{\gamma_{air}-1}{\gamma_{air}}} - 1 \right) \tag{10}$$

2.4.5 Turbine Efficiency and BSR

Figure 4 shows a spreading of the speed lines that relate efficiency to BSR, to be able to capture this, a turbocharger rotational speed dependent model has been adapted (11). The efficiency model consists of three sub-models, the first describing the relation between the maximum turbine efficiency and the turbine rotational speed (11b), the second describing the relation between the mechanical losses parameter c_m and rotational speed (11c), and the third describing the relation between BSR_{opt} and the rotational speed (11e). The models are found in Wahlström and Eriksson (2011), but the equations are slightly modified to take the spreading of the speed lines into account, also a max-selector used in Wahlström and Eriksson (2011) has been removed (in Equation 11c) to ensure continuous properties. To handle the loss of the switch, a boundary constraint is added to the optimization procedure, to make sure that the turbocharger speed never drops below the value of c_{22}.

$$N_{t,corr} = \frac{N_t}{\sqrt{T_{em}}} \tag{11a}$$

$$\eta_{tm}^{max} = c_{11} + c_{12} \left(\frac{N_{t,corr}}{10^5} \right)^2 \tag{11b}$$

$$c_m = c_{21} (N_{t,corr} - c_{22})^{c_{23}} \tag{11c}$$

$$BSR = \frac{r_t \omega_t}{\sqrt{2 c_{p,exh} T_{em} (1 - \Pi_t^{1-1/\gamma_{exh}})}} \tag{11d}$$

$$BSR_{opt} = c_{31} + c_{32} \left(\frac{N_{t,corr}}{10^5} \right)^{c_{33}} \tag{11e}$$

$$\eta_t = \eta_{tm}^{max} - c_m (BSR - BSR_{opt})^2 \tag{11f}$$

2.4.6 Compressor and Turbine Power

The turbine and compressor powers are described as in Eriksson and Nielsen (2014)

$$P_t \eta_t = \eta_t \dot{m}_t c_{p,exh} T_{em} \left(1 - \Pi_t^{1-1/\gamma_{exh}} \right) \tag{12a}$$

$$P_c = \frac{\dot{m}_c c_{p,air} T_{amb}}{\eta_c} \left(\Pi_c^{1-1/\gamma_{air}} - 1 \right) \tag{12b}$$

2.5 Controllable Flow Restrictors

2.5.1 Throttle Massflow

The throttle is described as an isentropic compressible restriction, the massflow through the throttle is dependent on the temperature T_{caf} and pressure p_{caf} before the throttle, and the pressure p_{im} after the throttle. Eriksson and Nielsen (2014) describes the model Equations (13). The model is linearized when the pressure ratio exceeds $\Pi_{lin} = 0.98$. At low pressure ratios the massflow increases, and eventually the flow reaches sonic velocity, which is reached at the critical pressure ratio Π_{thr}^{crit}.

$$\Pi_{thr}^{crit} = \left(\frac{2}{\gamma_{air}+1} \right)^{\frac{\gamma_{air}}{\gamma_{air}-1}} \tag{13a}$$

$$\Pi_{thr} = max \left(\frac{p_{im}}{p_{caf}}, \Pi_{thr}^{crit} \right) \tag{13b}$$

$$\Psi = \sqrt{\frac{2\gamma_{air}}{\gamma_{air}-1} \left(\Pi_{thr}^{\frac{2}{\gamma_{air}}} - \Pi_{thr}^{\frac{\gamma_{air}+1}{\gamma_{air}}} \right)} \tag{13c}$$

$$\Psi_{lin} = \sqrt{\frac{2\gamma_{air}}{\gamma_{air}-1} \left(\Pi_{lin}^{\frac{2}{\gamma_{air}}} - \Pi_{lin}^{\frac{\gamma_{air}+1}{\gamma_{air}}} \right) \frac{1-\Pi_{thr}}{1-\Pi_{lin}}} \tag{13d}$$

To handle the change in characteristics, happening at Π_{lin} and Π_{thr}^{crit}, two tangenshyperbolicus-based functions (tanhyp) are adapted to switch from 0 to 1 when the pressure ratios exceed Π_{lin} and Π_{thr}^{crit}. The main benefit of the tanhyp switch, compared to a conditional function, is that it holds the property of being continuously differentiable, which is a property desired by the optimal control software. Equations (13) and the *tanhyp* function forms the
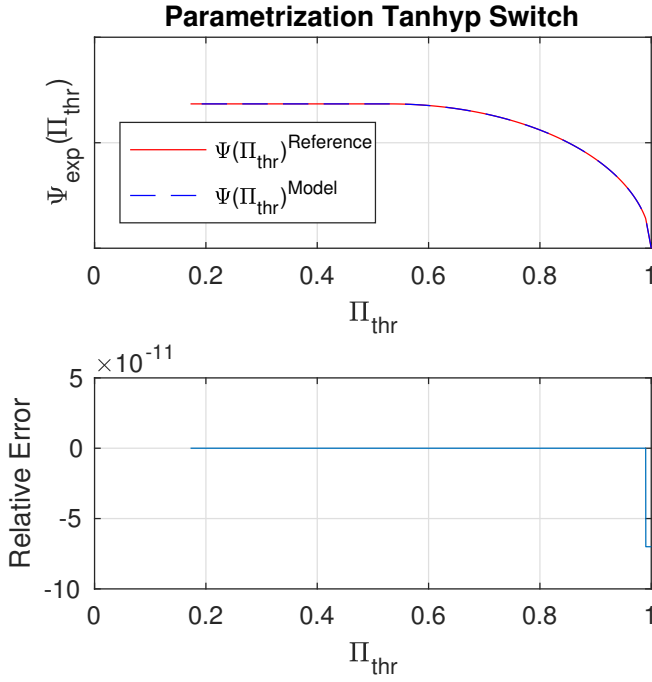
Figure 5. Model validation, the reference value of $\Psi_{exp}(\Pi_{thr})$ data (red) is compared with the tanhyp switch model output data (blue). The relative error when introducing the tanhyp switches are shown in the lower plot.

Figure 6. Model validation, the known throttle area (red) is compared with the model output data (blue).

following expressions for the flow condition Ψ_{exp} through the throttle

$$\Psi_{exp} = \Psi(\Pi_{thr}^{crit}) + f_{tanhyp,1}(-\Psi(\Pi_{thr}^{crit})$$
$$+ \Psi(\Pi_{thr}) + f_{tanhyp,2}(\Psi_{lin}(\Pi_{thr}) - \Psi(\Pi_{thr}))) \quad (14a)$$

$$f_{tanhyp,x}(\Pi_{thr}) = \frac{1 + tanhyp(c_{x1}(\Pi_{thr} - c_{x2}))}{2} \quad (14b)$$

The error introduced when using the tanhyp functions, compared to using a conditional function switching between the pressure ratio and the critical pressure ratio (13b), and the linearized and non-linearized flow equations (13c) and (13d), is shown in Figure 5.

The resulting massflow through the throttle is described as (Eriksson and Nielsen, 2014)

$$\dot{m}_{thr} = \frac{p_{caf}}{\sqrt{R_a T_{caf}}} C_d A_{thr}(u_{thr}) \Psi_{exp}(\Pi_{thr}). \quad (15)$$

No measurement data for different throttle positions was available (other than fully open), but the throttle area A_{thr} for different control signals u_{thr} was known and has been used to build the throttle model. The relation between the throttle area and the control signal is described by a fourth order equation (16), the result is displayed in Figure 6.

$$A_{thr} = c_1 u_{thr} + c_2 u_{thr}^4 \quad (16)$$

2.5.2 Wastegate Massflow

The model describing the wastegate massflow is developed in the same way as the throttle model (Equations
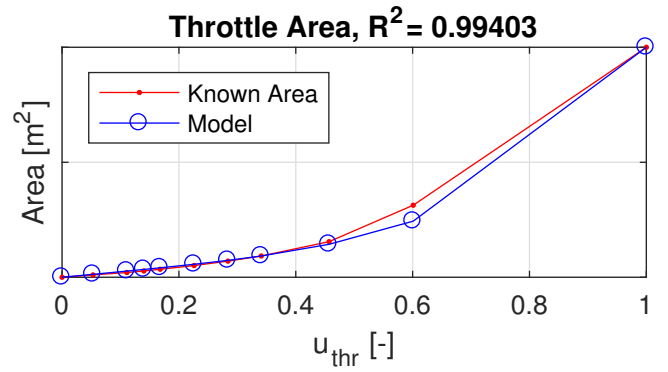
(13)-(16)) but with another area A_{wg}, and flow coefficient $C_{d,wg}$. The wastegate model is developed without the first tanhyp function in Equation (14a). There was no measurement of the wastegate massflow, the wastegate model is therefore used without any validation, other than making sure that the wastegate control signal is able to bypass massflow from the turbine. $C_{d,wg}$ is a scaling constant to ensure that the wastegate is working properly.

$$\dot{m}_{wg} = \frac{p_{em}}{\sqrt{R_a T_{em}}} C_{d,wg} A_{wg}(u_{wg}) \Psi_{exp}(\Pi_{wg}) \quad (17)$$

3 Optimal Control

To demonstrate the model's optimization and simulation capabilities an optimal control problem is solved. The optimization scenario is a so-called *tip-in*, this means transitioning the engine from a low load operating point to a high load operating point, essentially this corresponds to pushing the accelerator. Since no vehicle model is added, the tip-in is performed at constant engine speed, simply making a load increase. The problem is solved using a toolbox called YOP, using the direct collocation algorithm and NLP-solver IPOPT.

3.1 Objective

The optimization objective is to transition between the low load operation point to the high load operating point as fast as possible. This type of problem is interesting for investigating the performance boundaries of the engine. This can for instanced be used for analyzing the engine design, controller benchmarking, or comparing engine performance. In mathematical terms the objective function is formulated as

$$\min_{x(t),u(t)} t_f, \quad (18)$$

where t_f is the duration of the tip-in.

3.2 Model Constratints

To restrict the optimization to meaningful solutions, constraints need to be introduced. The most basic of these are the model constraints:

$$\dot{x}(t) = f(x(t), u(t)) \tag{19a}$$
$$x_{min} \leq x(t) \leq x_{max} \tag{19b}$$
$$u_{min} \leq u(t) \leq u_{max} \tag{19c}$$
$$0 \leq \phi(t) \leq 1/\lambda_{min} \tag{19d}$$
$$BSR_{min} \leq BSR(t) \leq BSR_{max} \tag{19e}$$
$$\dot{m}_c(t) \geq \dot{m}_{zsl}(N_t) \tag{19f}$$
$$\dot{m}_c(t) \leq \dot{m}_{ch}(N_t) \tag{19g}$$
$$N_t(t) \geq c_{22} \text{ (from Equation (11c))} \tag{19h}$$
$$N_e(t) = N_{e,fixed} \tag{19i}$$

The first constraint (19a) says that the state must follow the system dynamics, the second (19b) and third (19c) that the state and control must be operated within their limits, the fourth (19d) that the air-to-fuel equivalence ratio (expressed as the fuel-to-air equivalence ratio in $\phi(t)$ to avoid the singularity when no fuel is injected) must be above the smoke limit, the fifth (19e) that the turbine blade-speed-ratio must be within its bounds, the sixth (19f) and seventh (19g) that the compressor must stay below surge and above choke massflow, and the eight (19h) that the turbocharger speed should be above the value of the c_{22} parameter (from Equation (11c)), and the ninth (19i) that the engine speed is fixed at $N_{e,fixed}$. The sixth (19f) and seventh (19g) constraints are illustrated in Figure 7, where the red line represents the surge line and the green the choke line.

3.3 Boundary Constraints

To setup the tip-in scenario, boundary constraints defining the initial and terminal operating conditions of the optimization are introduced

$$x(0) = x_0 \tag{20a}$$
$$u(0) = u_0 \tag{20b}$$
$$M_e(t_f) = M_{e,des}, \tag{20c}$$

where x_0 and u_0 define the initial operating point, and $M_{e,des}$ the desired engine torque. When the desired torque is reached, the tip-in is completed.

3.4 Numerical Solution

The numerical solution to the optimal control problem was found using an open-source software called YOP. For the solution presented in the paper the direct collocation algorithm was used, using 9 Legendre points in each collocation interval. The control signal was discretized into 90 equidistant segments on which the control was parameterized as constant, making it piecewise constant over the entire time horizon. The resulting NLP from the direct collocation algorithm was solved using IPOPT.

4 Results

The optimal control problem was parameterized in such a way that the engine was running at 1300 RPM, starting
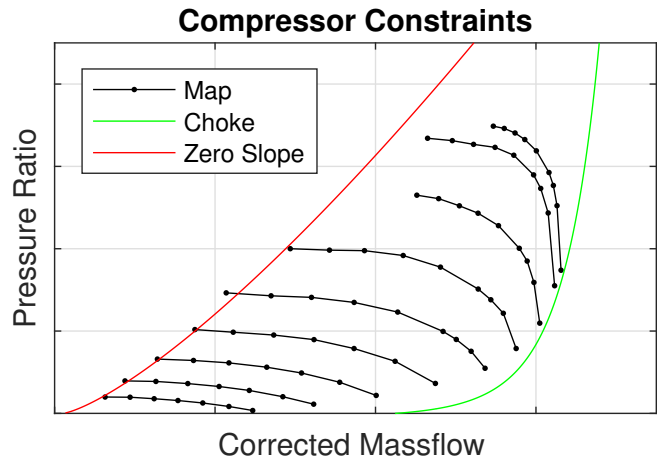

Compressor Constraints

Figure 7. Compressor constraints. The minimum massflow bound is drawn in red and called the zero slope line. The maximum massflow bound is drawn in green and called the choke line. The black lines are speed lines from the compressor map.

at 15 Nm and required to reach 1800 Nm. The minimum time of doing this is 2.95 s, which is seen in the top plot of Figure 8. In Figures 9 and 10 the state and control trajectories are shown, in Figure 8 interesting internal system variables are shown, and in Figure 11 the turbocharger behavior can be studied from a turbo map perspective. Trivially, it takes oxygen to combust fuel, this is however what limits the tip-in performance. Looking at the bottom plot of Figure 8, it is seen that the minimum value of the fuel-to-air equivalence ratio λ_{min} is an active constraint as soon as the engine begins to increase the load. λ_{min} is set close to, but above 1 (below $\lambda = 1$ there is too little oxygen to burn all the fuel), which prevents smoke formation. However, even without this constraint there is still not enough air to be able to combust the necessary amount of fuel to produce the requested torque. To increase the air massflow, the compressor rotational speed needs to be increased in order to change the operating point. What restricts the transition time is the turbocharger inertia. Since it restricts how fast the compressor can change operating point, it consequently also restricts the entire engine's response time, limiting the tip-in performance.

Looking at the optimal control trajectories in Figure 10, the trajectories are predictable and intuitive. The fuel injection follows the smoke limit, the throttle stays open, and the wastegate is kept closed right until the end where it opens fully. The reason for the wastegate to open at the end, is that it decreases the pumping loss, this can be seen in the middle plot of Figure 8. For the presented parametrization of the problem, the engine is not required to be in a steady-state condition at the terminal boundary, which is why it opens the wastegate fully and not just partly.

The results shows that the model behaves in an intuitive way, which indicates that the model is physically sound and that it is suitable for simulation and optimization studies.
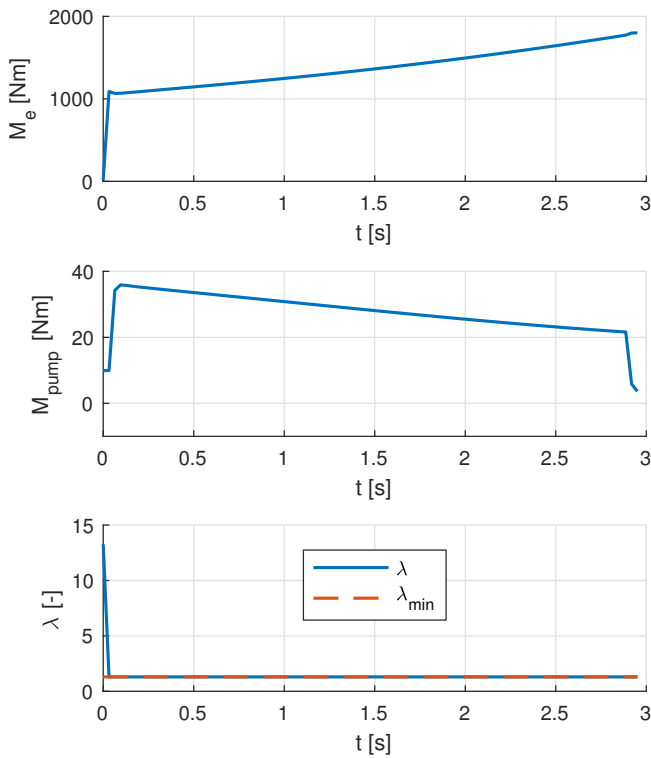
Figure 8. Internal system variables during tip-in. At the top, the engine torque is shown, in the middle the pumping torque, and at the bottom the air-to-fuel equivalence ratio.
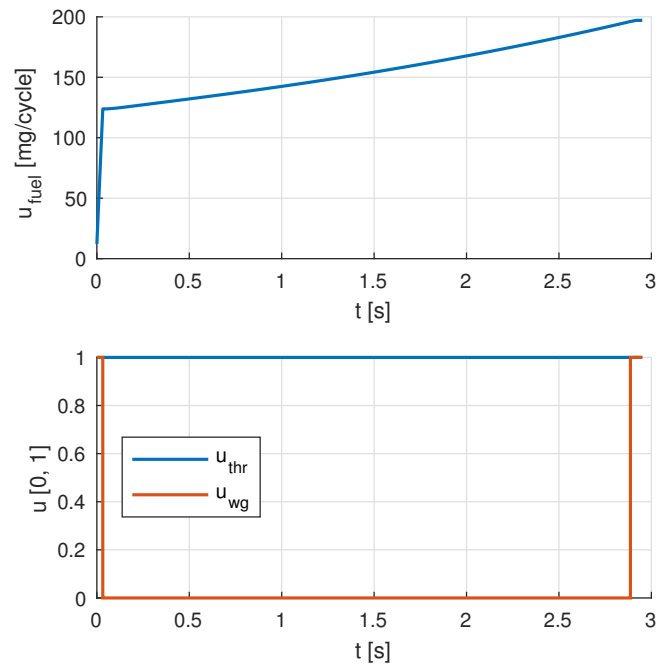

Figure 10. Tip-in control trajectories. At the top, fuel injection is seen, and at the bottom throttle and wastegate control are seen.
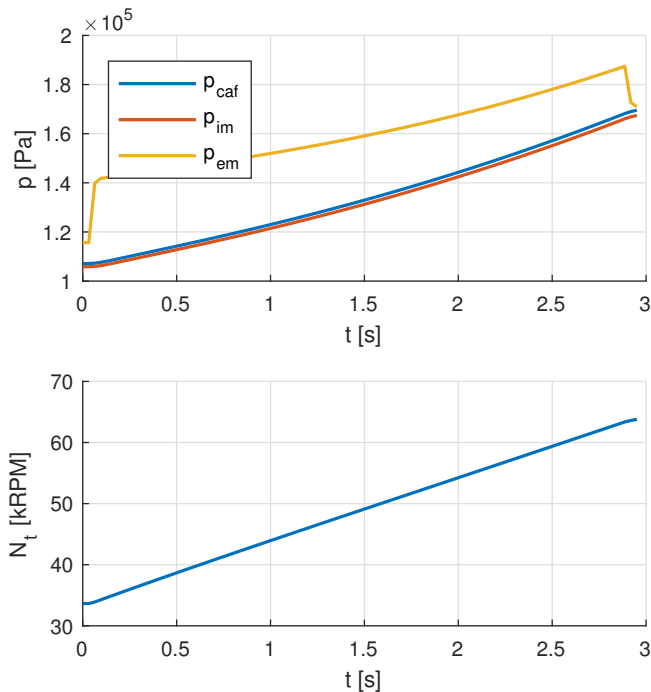

Figure 9. Tip-in state trajectories. Top plot showing the pressure states, and the bottom plot showing the turbocharger speed.
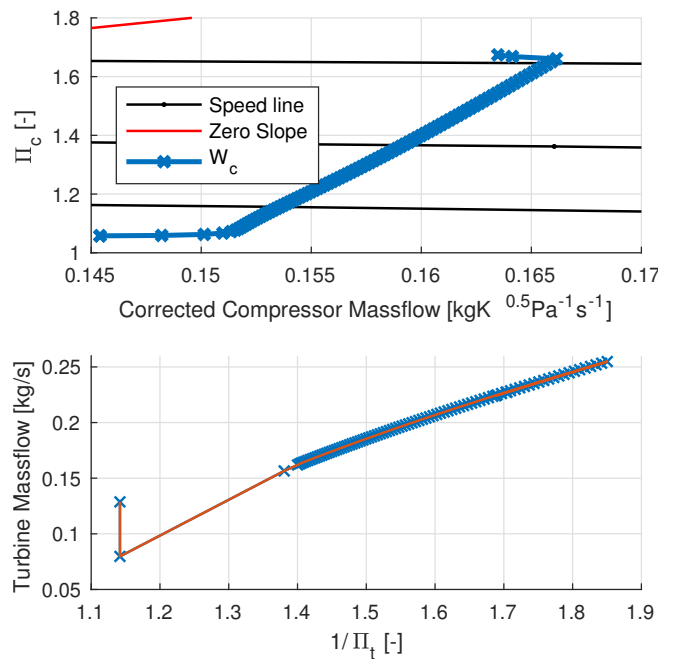

Figure 11. Tip-in turbocharger behaviour. Top plot showing the compressor behavior in the compressor map, and bottom plot showing the turbine behavior in the turbine map.

5 Conclusions

This paper has:

- Developed and validated a model of a turbocharged heavy-duty diesel engine equipped with throttle and wastegate.

- Developed a component based model, to make it easily adjustable for future use and further development.

- Shown, using optimization, that the model behaves in a sound and intuitive way, strongly indicating that it is suitable for optimization and simulation studies.

References

Joel Andersson. *A General-Purpose Software Framework for Dynamic Optimization*. PhD thesis, Arenberg Doctoral School, KU Leuven, Department of Electrical Engineering (ESAT/SCD) and Optimization in Engineering Center, Kasteelpark Arenberg 10, 3001-Heverlee, Belgium, October 2013.

Jonas Asprion. *Optimal Control of Diesel Engines: Modeling, Numerical Methods and Applications*. PhD thesis, ETH Zürich, Sonneggstrasse 3, CH-8092 Zurich, Switzerland, 2013.

John T. Betts. *Practical Methods for Optimal Control and Estimation Using Nonlinear Programming*. SIAM, second edition, 2010.

Lorenz T. Biegler. *Nonlinear Programming: Concepts, Algorithms, and Applications to Chemical Processes*. MOS-SIAM Series on Optimization, 2010.

Lars Eriksson and Lars Nielsen. *Modeling and Control of Engines and Drivelines*. John Wiley and Sons Ltd, 2014.

Fiona Harvey. Four of world's biggest cities to ban diesel cars from their centres. The Guardian, 2 December 2016. https://www.theguardian.com/environment/2016/dec/02/four-of-worlds-biggest-cities-to-ban-diesel-cars-from-their-centres.

Viktor Leek, Kristoffer Ekberg, and Lars Eriksson. Development and Usage of a Continuously Differentiable Heavy Duty Diesel Engine Model Equipped with VGT and EGR. *SAE Technical Paper*, 2017.

Oskar Leufvén and Lars Eriksson. A surge and choke capable compressor flow model—validation and extrapolation capability. *Control Engineering Practice*, 21(12):1871 – 1883, 2013. ISSN 0967-0661. doi:http://dx.doi.org/10.1016/j.conengprac.2013.07.005. URL http://www.sciencedirect.com/science/article/pii/S0967066113001354.

Vaheed Nezhadali and Lars Eriksson. Optimal control of a diesel-electric powertrain during an up-shift. In *SAE 2016 World Congress, paper number 2016-01-1237*, 2016.

Martin Sivertsson. *Optimal Control of Electrified Powertrains*. PhD thesis, Linköping University, Sweden, 2015.

Martin Sivertsson and Lars Eriksson. An optimal control benchmark: Transient optimization of a diesel-electric powertrain. In *SIMS 2014 - 55th International Conference on Simulation and Modelling*, Aalborg, Denmark, 2014.

Pål Skogtjärn. Modelling of the exhaust gas temperature for diesel engines. Master's thesis, Linköpings Universitet, SE-581 83 Linköping, 2002.

Vaclav Smil. *Prime Movers of Globalization*. MIT Press, July 2010.

J Wahlström and L Eriksson. Modelling diesel engines with a variable-geometry turbocharger and exhaust gas recirculation by optimization of model parameters for capturing non-linear system dynamics. *Proceedings of the Institution of Mechanical Engineers, Part D: Journal of Automobile Engineering*, 225(7):960–986, 2011. doi:10.1177/0954407011398177. URL http://dx.doi.org/10.1177/0954407011398177.

Wächter, Andreas and Biegler, Lorenz T. On the implementation of a primal-dual interior point filter line search algorithm for large-scale nonlinear programming, 2006.